JOURNAL OF Applied Polymer SCIENCE

Comparison of Covalent and Noncovalent Interactions of Carbon Nanotubes on the Crystallization Behavior and Thermal Properties of Poly(3-hydroxybutyrate-*co*-3-hydroxyvalerate)

Hou-Yong Yu,[1,2] Ju-Ming Yao,[1] Zong-Yi Qin,[2] Lin Liu,[1] Xiao-Gang Yang[1]

[1]Key Laboratory of Advanced Textile Materials and Manufacturing Technology, Ministry of Education, College of Materials and Textile, Zhejiang Sci-Tech University, Hangzhou 310018, China

[2]State Key Laboratory for Modification of Chemical Fibers and Polymer Materials, College of Materials Science and Engineering, Donghua University, Shanghai 201620, China

Correspondence to: J.-M. Yao (E-mail: yaoj@zstu.edu.cn) or Z.-Y. Qin (E-mail: phqin@dhu.edu.cn)

ABSTRACT: In this study, multiwalled carbon nanotubes (MWCNTs) were dispersed into a poly(3-hydroxybutyrate-*co*−3-hydroxyvalerate) (PHBV) matrix, in which PHBV was either covalently attached to the nanotubes through an esterification reaction between the carboxylic groups of functionalized MWCNTs and the hydroxyl groups of PHBV with toluene diisocyanate as a coupling agent or physically mixed to result in only noncovalent interactions. The structure, crystallization behavior, and thermal properties of the resulting nanocomposites were studied. We found that the crystallization of PHBV grafted onto the MWCNTs (PHBV-*g*-MWCNTs) was markedly hindered and exhibited an exothermic peak caused by cold crystallization, whereas the nonisothermal crystallization of PHBV was enhanced because a heterogeneous nucleation effect appeared in the PHBV/MWCNTs. Moreover, the maximum decomposition temperature of the PHBV-*g*-MWCNTs was improved by about 14.4°C compared with that of the PHBV/MWCNTs and by about 23.7°C compared with that of the original PHBV. Furthermore, the PHBV-*g*-MWCNTs exhibited the wider melt-processing window than the PHBV/MWCNTs and original PHBV. © 2013 Wiley Periodicals, Inc. J. Appl. Polym. Sci. 130: 4299–4307, 2013

KEYWORDS: biopolymers and renewable polymers; crystallization; grafting; graphene and fullerenes; nanotubes; thermal properties

Received 19 January 2013; accepted 8 May 2013; Published online 17 July 2013
DOI: 10.1002/app.39529

INTRODUCTION

Poly(3-hydroxybutyrate)-*co*-(3-hydroxyvalerate) (PHBV), which is a truly biodegradable polymer, has been recognized as a potential environmentally friendly substitute for traditional plastics such as polyethylene and polystyrene. PHBV is a well-known biodegradable aliphatic polyester, and its various properties, including its as natural origin, biodegradability, biocompatibility, nontoxicity, piezoelectricity, and thermoplasticity, make it suitable for a variety of applications in biomedical and pharmaceutical applications, such as tissue engineering and drug-delivery systems.[1–4] Many studies have been conducted with poly(3-hydroxybutyrate-*co*−3-hydroxyvalerate) and PHBV as biomaterials for *in vitro* and *in vivo* studies.[5–7] However, the practical application of PHBV has been limited by some drawbacks, including its narrow melt-processing window due to a low thermal decomposition temperature and high melting temperature and its relative difficulty in degrading in the body because of its high crystallinity (X_c).[8–10] Therefore, nanoscale reinforcements of these biodegradable polymers with organic or inorganic nanofillers with covalent or noncovalent approaches may be an effective way to improve these properties. Carbon nanotubes (CNTs), with their exceptional electrical and mechanical properties, have been becoming more and more attractive as ideal reinforcing materials for nanocomposites because the thermal and mechanical properties of the polymeric matrix can be enhanced largely by the introduction of a small amount of CNTs.[11–15]

Recently, many attempts have been made to improve the crystallization behavior and thermal and mechanical properties of poly(3-hydroxybutyrate-*co*−3-hydroxyvalerate) or PHBV through physical blending with CNTs.[8–10,12,16,17] Lai et al.[8] reported PHBV/multiwalled carbon nanotubes (MWCNTs) composites prepared by a solution process. Their calorimetric measurements of the nanocomposites indicated that the crystallization rate and crystallization temperature increased with the addition of MWCNTs. The thermal degradation temperature increased from 255°C for PHBV to 271°C for the composite with 2 wt % MWCNTs. Shan et al.[16] also found that well-dispersed MWCNTs acted as an effective heterogeneous nucleation agent in the PHBV matrix to induce an increase X_c and the crystallite size. The crystallization peak temperatures (T_c's)

continuously increased from 81.9 to 111.4°C with increasing MWCNT contents from 0 to 7 wt %. In addition, the addition of CNTs had a twofold effect on the crystallization of PHBV, accelerating the nucleation rate while retarding the following crystal growth rate, but on the whole, the overall crystallization rate of PHBV improved largely. These different phenomena were found in the PHBV/MWCNT nanocomposites reported by Sanchez-Garcia et al.[12] They found that the glass-transition temperature of PHBV increased with increasing CNT content; this indicated that the CNTs hindered the crystallization process of PHBV; they explained that the filler dispersion and interfacial adhesion could hinder, to some extent, the polymer chain lateral rearrangement and, hence, crystallization in the nanocomposites. As shown by these studies, the property enhancement of PHBV/CNT nanocomposites is strongly dependent on the nanocomposite preparation, the dispersion state of the CNTs, and interfacial interaction between the CNTs and the polymer matrix. For noncovalent approaches, bulk CNTs incorporated into a polymer matrix tend to form aggregates because of the relatively poor interfacial interaction between them and thus do not guarantee property enhancements in the nanocomposites.[11,14,15] It is well known that good interfacial adhesion between the CNTs and the polymer matrix is essential for efficient load transfer in nanocomposites. High-performance nanocomposites demand not only the uniform dispersion of the CNTs in the polymer matrix without aggregation but also strong CNT/polymer matrix interactions.[14,15] Graft polymerization as a simple and powerful covalent approach can prevent this aggregation phenomenon of CNTs, confine the crystal structure and, especially, form covalent bonding between the matrix and CNTs, which constitutes the strongest type of interfacial bonding;[13] these modified CNTs can also act as reinforcing fillers in the nanocomposites without consideration of the miscibility between the grafting polymer and the polymer matrix.

To the best of our knowledge, the grafting of PHBV onto CNTs has not been reported so far. It is of great importance and interest to study the crystallization behavior of biodegradable polymers because it affects not only the crystalline structure and morphology of semicrystalline polymers but also their final physical properties and biodegradability. In this study, the effects of the covalent and noncovalent interactions of CNTs on the crystallization behavior and thermal properties of PHBV-based composites were investigated because polymer processing is usually performed under nonisothermal conditions, and the crystallization behavior and thermal degradation behavior can provide useful information about the determination of the optimum processing conditions and the identification of potential applications of the final products. Therefore, PHBV was grafted onto MWCNTs through an esterification reaction between the carboxylic groups of the functionalized MWCNTs and hydroxyl groups of PHBV with toluene diisocyanate (TDI) as a coupling agent. A comparison study of the PHBV/MWCNTs containing 3 wt % MWCNTs was prepared by solution casting. The influence of the interaction types (covalent or noncovalent) on the crystallization behavior and thermal stability of the composites was evaluated directly.

EXPERIMENTAL

Materials

Commercial PHBV (number-average molecular weight = 5.90×10^4, weight-average molecular weight/number-average molecular weight = 3.18 and Hydroxyvalerate (HV) = 2.57 mol %) was purchased from Tiannan Biological Material Co., Ltd. (Ningbo, China) and was purified by precipitation in ethanol from a chloroform solution. Commercial MWCNTs [purity = 95 wt %, diameter = 20–40 nm, length = 5–15 μm, chemical vapor deposition (CVD) method] were purchased from Shenzhen Nanotech Port. Co., Ltd. (Shenzhen, China). TDI, acetone, *N,N*-dimethyl formamide (DMF), sulfuric acid (H_2SO_4), nitric acid (HNO_3), ethanol (99.8%), diglyme, ethylene glycol, and dibutyl tin dilaurate (90.0%) were purchased from Guoyao Group Chemical Reagent Co., Ltd. All reagents and solvents were used as received or purified with standard procedures.

Nanocomposite Preparation

To remove the impurities, the MWCNTs were treated with a mixture of concentrated sulfuric and nitric acids (3:1 v/v) under ultrasonic irradiation at 70°C for 3 h. After the mixture was cooled to room temperature, it was diluted with deionized water and then vacuum-filtered through a 0.22-mm Millipore polypropylene membrane and washed with distilled water until the pH value of the filtrate was about 7. The filtered solid was dried *in vacuo* for 24 h at 60°C to give carboxyl-functionalized multiwalled carbon nanotubes (MWCNT-COOHs).

Telechelic OH-terminated poly(3-hydroxybutyrate-*co*−3-hydroxyvalerate) (PHBV-OH) was prepared by a transesterification procedure similar to our previously reported method,[18,19] and the reaction is illustrated in Scheme 1. The detailed synthesis process was as follows: 30 g of PHBV and 300 mL of diglyme were placed in a four-necked, round-bottomed flask with a mechanical stirrer under a nitrogen atmosphere. Then, the flask was heated to 140°C in an oil bath with continuous mechanical stirring. After PHBV was dissolved completely, 60 mL of ethylene glycol and 0.3 g of dibutyl tin dilaurate as a catalyst were quickly added to the flask. After a desired reaction time of 7.5 h, the products were precipitated with ethanol, washed repeatedly with ethanol, and dried *in vacuo*. The molecular weight of PHBV-OH was about 1980 g/mol as measured by gel permeation chromatography.[18,19]

The PHBV nanocomposites were prepared by two different methods: One method was the physical mixture of PHBV through a solution casting method, and the MWCNT-COOHs (3 wt %) in DMF at room temperature under ultrasonic irradiation (PHBV/MWCNTs), in which only noncovalent interaction occurred. Another was the grafting of PHBV in the surface of MWCNTs through the esterification reaction between carboxylic groups of the purified MWCNT-COOHs and hydroxyl groups of PHBV-OH with TDI as a coupling agent via the synthetic pathway, as shown in Scheme 1 (PHBV-*g*-MWCNTs). In a typical reaction, the purified MWCNT-COOHs were allowed to swell in 150 mL of DMF in a 250-mL, four-necked, round-bottom flask. The swollen MWCNT-COOHs were sonicated for 30 min in an oil bath for 1 h, and then, 5 mL of TDI was subsequently added to the flask for 1 h under a nitrogen atmosphere. Subsequently, 3.0 g of PHBV was added to the flask, and the flask was heated to 70°C with continuous mechanical

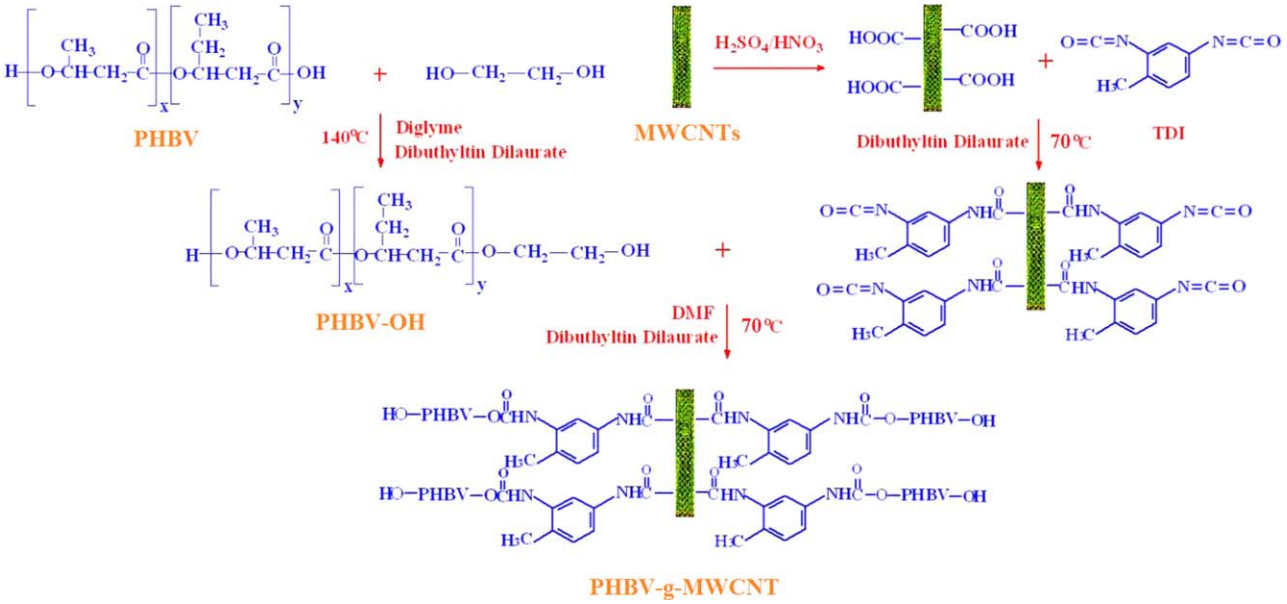

Scheme 1. Whole synthesized process of the PHBV-*g*-MWCNTs. [Color figure can be viewed in the online issue, which is available at wileyonlinelibrary.com.]

stirring. After a desired reaction time of 3 h, the resulting products were filtered through a 0.22-μm polycarbonate membrane, washed with acetone several times, collected through filtration, and dried at 60°C *in vacuo* overnight. The residual noncovalently attached PHBV dissolved in acetone was removed from the mixture via filtration.

Characterization

The morphologies of the functionalized MWCNTs, PHBV/MWCNTs, and PHBV-*g*-MWCNTs were observed by field emission scanning electron microscopy (FESEM; Hitachi S-4800). The structures of PHBV, PHBV/MWCNTs, and PHBV-*g*-MWCNTs were characterized by a Fourier transform infrared (FTIR) spectrometer (Nicolet Nexus 6700), and a total of 32 scans at a resolution of 4 cm^{-1} were recorded for each sample at room temperature. Spherulitic morphologies were observed by a polarized optical microscope (Olympus BX51) with a temperature controller (Linkam THMS 600). A thin film of each sample was pressed between two glass slides, kept at 190°C for 2 min on hot stage, and then cooled to 45°C quickly (at a rate of 50°C/min). The images of spherulites were recorded by a digital camera (Nikon), and the radius of the spherulites was measured as a function of the crystallization time. The crystal structures were determined on a wide-angle X-ray diffraction (WAXD) instrument (Rigaku D/Max-2550 PC).

The crystallization behavior and melting behavior of the PHBV, PHBV/MWCNTs, and PHBV-*g*-MWCNTs were characterized by a differential scanning calorimetry (DSC; MDSC TA-2910). Nitrogen was used as the purge gas at a flow rate of 40 mL/min for the DSC cell. Samples of about 10 mg were weighed and sealed in an aluminum DSC pan and placed in a DSC cell. They were first heated from 0 to 200°C at a rate of 20°C/min. The samples were kept at 200°C for 5 min to eliminate the previous heat history and subsequently cooled to 0°C at rates of 2, 5, 10, and 20°C/min (the first cooling traces); then, they were heated to 200°C (the second heating traces) at rates of 2, 5, 10, and 20°C/min, respectively. Crystallization peak temperature (T_c), which was obtained from the first cooling traces. $T_{c(\text{onset})}$, which was called onset of crystallization was the temperature at the intercept of the tangents at the baseline and the high-temperature side of the exotherm. The initial slope of the exotherm (S_i), defined as the nucleation rate, was the slope at inflexion on the high-temperature side of the exothermic in the first cooling traces. The greater the S_i was, the greater the nucleation rate was. The melting behaviors were studied from the second heating traces. To evaluate the thermal stability, thermogravimetric analysis (TGA) was carried out with a Netzsch TG 209 F1 TGA instrument coupled with quadrupole mass spectrometer (QMS). The samples were heated from room temperature to 500°C at a heating rate (β) of 20°C/min under a dynamic nitrogen atmosphere with a flow rate of 30 mL/min.

RESULTS AND DISCUSSION

Chemical Structure

The structures of the neat PHBV, PHBV/MWCNT and PHBV-*g*-MWCNTs were characterized by FTIR spectra, as shown in Figure 1. The bands around 3016–2960, 2949–2929, and 2888–2867 cm^{-1} were assigned to CH_3 asymmetric stretching modes, CH_2 antisymmetric stretching modes, and CH_3 symmetric stretching modes, respectively. The carbonyl stretching band of the as-received PHBV could be resolved into an intensive band at 1724 cm^{-1} and a weak shoulder at 1740 cm^{-1} [as shown in Figure 1(b)]; these corresponded to the carbonyl stretching bands of the crystalline and amorphous regions, respectively.[18] The bands in the range 1500–800 cm^{-1} due to the CH_3 and CH bending vibrations and the C—O—C and C—C stretching vibrations heavily overlapped. Compared to those characteristics for neat PHBV, a new absorbance band at

Applied Polymer SCIENCE

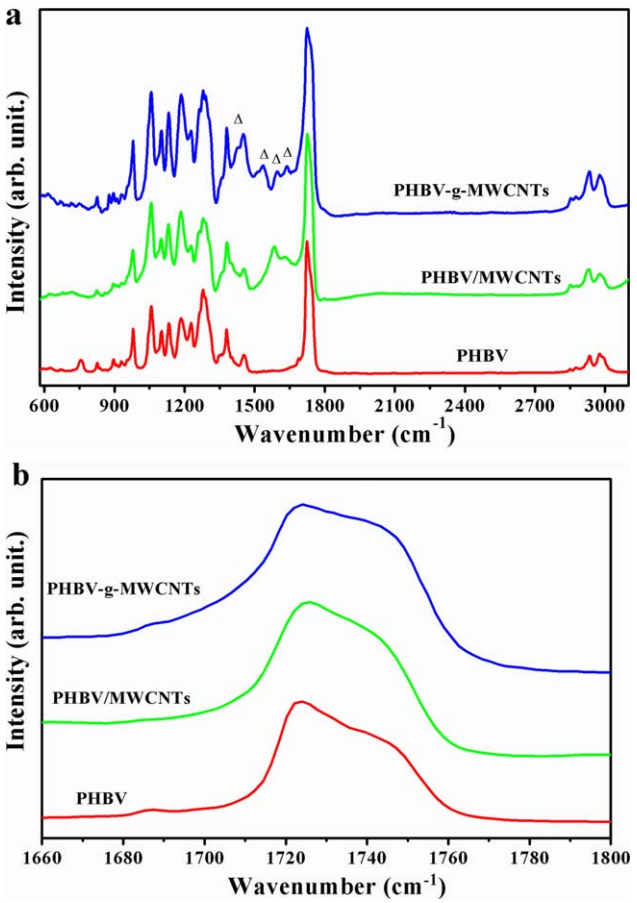

Figure 1. (a) FTIR spectra and (b) absorption bands in the region of C═O stretching vibrations for the neat PHBV, PHBV/MWCNTs, and PHBV-*g*-MWCNTs. [Color figure can be viewed in the online issue, which is available at wileyonlinelibrary.com.]

1583 cm^{-1} corresponded to the carboxylic group (—O—C═O—) antisymmetric stretching modes of the MWCNT-COOHs from PHBV/MWCNTs, but no obvious carboxylic absorbance band was found in the PHBV-*g*-MWCNTs. This could have been because the carboxylic groups of the MWCNT-COOHs were reacted with the isocyanate (NCO) groups of TDI and formed the amide groups (—NH—CO—) in the PHBV-*g*-MWCNTs, as shown in Scheme 1. These amide group stretching bands appeared around 1537 and 1639 cm^{-1}. The bands corresponded to the ring vibrational modes of the bound phenyl group appearing around 1452 and 1597 cm^{-1}. These new bands are denoted by open triangles in Figure 1(a). These results indicate that the PHBV molecules were successfully covalently bonded to the MWCNTs through TDI as a coupling agent. In addition, compared to neat PHBV, the crystalline-sensitive peaks of PHBV at 1277 and 1262 cm^{-1} (C—O—C stretching mode) clearly became stronger in the PHBV/MWCNT composite. For PHBV-*g*-MWCNTs, the intensity of the amorphous state of the C═O stretching band at 1740 cm^{-1} and C—O—C stretching band near 1183 cm^{-1} increased. These results indicated that the crystallization of the PHBV component was enhanced by the presence of the MWCNTs, but the amorphous phase of the PHBV component in the PHBV-*g*-MWCNTs increased.

Morphologies

Figure 2 shows the FESEM images of the functionalized MWCNTs, PHBV/MWCNTs, and PHBV-*g*-MWCNTs. As shown in Figure 2(b), there was no apparent aggregation of the MWCNT-COOHs in the PHBV matrix. Meanwhile, we also observed that most of the MWCNT-COOHs remained curved in shape or even interwoven in the nanocomposite because of the extreme flexibility of the nanotubes. The uniformly dispersed bright dots and lines indicate the ends of the broken MWCNT-COOHs and show that a fine dispersion of the MCWNT-COOHs embedded into PHBV matrix could be achieved by the presence of the carboxyl groups of the MWCNTs. As shown in Figure 2(c), compared with the functionalized MWCNTs, we found that the PHBV-*g*-MWCNTs had a clear core–shell structure composed of MWCNTs with an

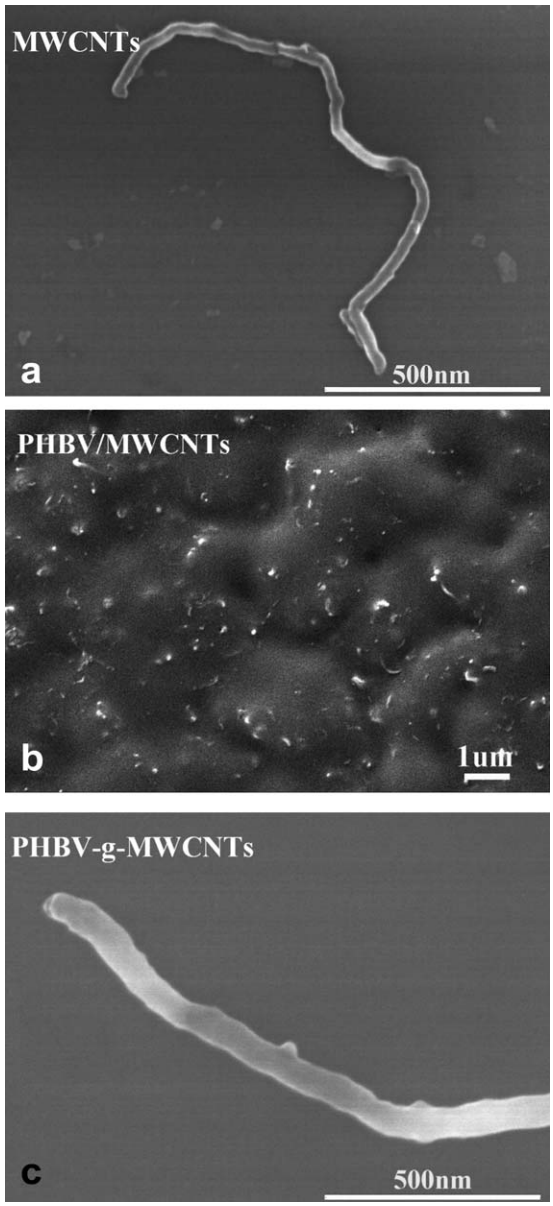

Figure 2. FESEM images of the functionalized MWCNTs, PHBV/MWCNTs, and PHBV-*g*-MWCNTs.

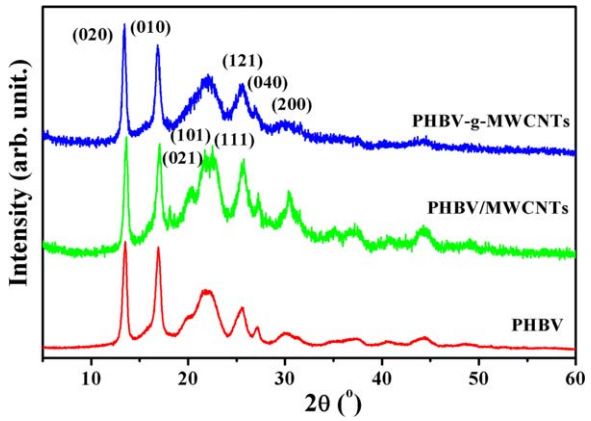

Figure 3. WAXD patterns of the neat PHBV, PHBV/MWCNTs, and PHBV-*g*-MWCNTs. [Color figure can be viewed in the online issue, which is available at wileyonlinelibrary.com.]

average diameter of 30 nm as a hard core and a PHBV layer with an average thickness of 60 nm as a soft shell. This result implies that PHBV layer successfully covered the surface of the MWCNTs.

Crystalline Structure

The WAXD diffractograms of the neat PHBV, PHBV/MWCNTs, and PHBV-*g*-MWCNTs displayed typical diffraction patterns of the α form, and all of the samples were semicrystalline materials, as shown in Figure 3. A comparison of the spectrum of the neat PHBV with that of the PHBV/MWCNTs showed a new diffraction peak at 18.2° with 0.482-nm *d*-spacing in the WAXD patterns of PHBV/MWCNTs; this was a characteristic diffraction peak for the *β* form with a planar zigzag conformation (from pseudohexagonal system) of PHBV.[20–22] This result indicates that noncovalent interactions of the MWCNTs influenced the mechanism of nucleation or the growth of the PHBV crystals. The possible mechanism will be explored in our future work. Moreover, the three main peaks located around 20.2, 21.6, and 22.4° were assigned to (021), (101), and (111) planes of PHBV, respectively. The intensity of these peaks in the PHBV/MWCNTs was stronger than those in the original PHBV; meanwhile, there was a sharp rise in the intensity of the characteristic peaks (200) at 30.4° in the PHBV crystals in the PHBV/MWCNT composite. This could be ascribed to the preferential crystallite growth of PHBV along the direction of the α axis. A similar phenomenon was found in a previous study.[6] However, for the PHBV-*g*-MWCNTs, a decrease in the intensity of the characteristic (021), (101), and (200) peaks was observed; this implied that the crystallite growth of PHBV with the covalent interactions of the MWCNTs along the direction of the α axis was inhibited. In addition, the X_c values of the neat PHBV, PHBV/MWCNTs, and PHBV-*g*-MWCNTs are listed in Table I. We found that the X_c of the PHBV-*g*-MWCNTs was only 51.3%; this was a decrease of more than 11% compared with that of the PHBV/MWCNTs and a decrease of about 6.8% compared with that of neat PHBV. These results indicate that the MWCNTs could act as nucleating agents to improve crystallization of PHBV and form perfect crystals; this resulting in a higher X_c. However, the reverse situation was found for the PHBV-*g*-MWCNTs because of the covalent interaction of the MWCNTs on PHBV.

Nonisothermal Crystallization and Melting Behavior

It is well known that X_c plays an important role in the physical properties and biodegradability of the biodegradable polymers. Therefore, the nonisothermal crystallization and melting behavior of the neat PHBV, PHBV/MWCNTs, and PHBV-*g*-MWCNTs were investigated to understand the effect of the covalent and noncovalent interactions of the MWCNTs on the crystallization behavior of PHBV. It was shown from Figure 4(a) that S_i of the PHBV/MWCNTs was higher than that of original PHBV; this implied that the nucleating rate of the PHBV/MWCNTs was greater than that of the original PHBV. This indicated an efficient heterogeneous nucleation of the MWCNTs for facilitating the PHBV crystallization. In Figure 4(a), the crystallization peaks appeared for the PHBV and PHBV/MWCNTs, but no crystallization peak was found in the PHBV-*g*-MWCNTs. T_c increased from 64.7°C for PHBV to 94.8°C for the PHBV/MWCNTs; this indicated that the crystallization of the PHBV/MWCNTs became easier probably because the CNT-modified chains were more nucleating for PHBV crystallization. A similar behavior was reported in the comparison of the thermal properties of PHBV and its composite containing 2 wt % MWCNTs; this indicated that the MWCNTs could act as nucleating agents and facilitate the heterogeneous crystallization traces.[8] The parameters of the crystallization process of the original PHBV and PHBV/MWCNTs are shown in Figure 4(a), The parameter $T_{c(\text{onset})} - T_c$ was a measure of the overall rate of crystallization.[19] The smaller the $T_{c(\text{onset})} - T_c$ was, the greater the rate of crystallization was. We observed that $T_{c(\text{onset})} - T_c$ of PHBV/MWCNTs decreased from 21.3°C (original PHBV) to 19.2°C; this revealed that the crystallization rate of the PHBV/MWCNTs was larger than that of the original PHBV.

As shown in Figure 4(b), we found that the double melting peaks around 140°C appeared in all of the samples during the

Table I. Parameters for the Thermal Stability of the Neat PHBV, PHBV/MWCNTs, and PHBV-*g*-MWCNTs

Sample	X_c (%)	T_{m2} (°C)	T_0 (°C)	$T_{5\%}$ (°C)	T_{max} (°C)	T_f (°C)	$T_0 - T_{m2}$ (°C)
PHBV	58.1	143.7	251.5	231.7	265.5	268.7	107.8
PHBV/MWCNTs	62.2	149.6	262.2	242.3	274.8	283.1	112.6
PHBV-*g*-MWCNTs	51.3	141.5	270.8	249.7	289.2	301.6	129.3

X_c was calculated from the WAXD patterns. The values of T_{m2} were calculated from the DSC curve at the second heating scans. The values of T_0, $T_{5\%}$, T_{max}, and T_f were calculated from the TGA curve at a *β* of 10°C/min. $T_0 - T_{m2}$ represents the melt-processing window.

Applied Polymer SCIENCE

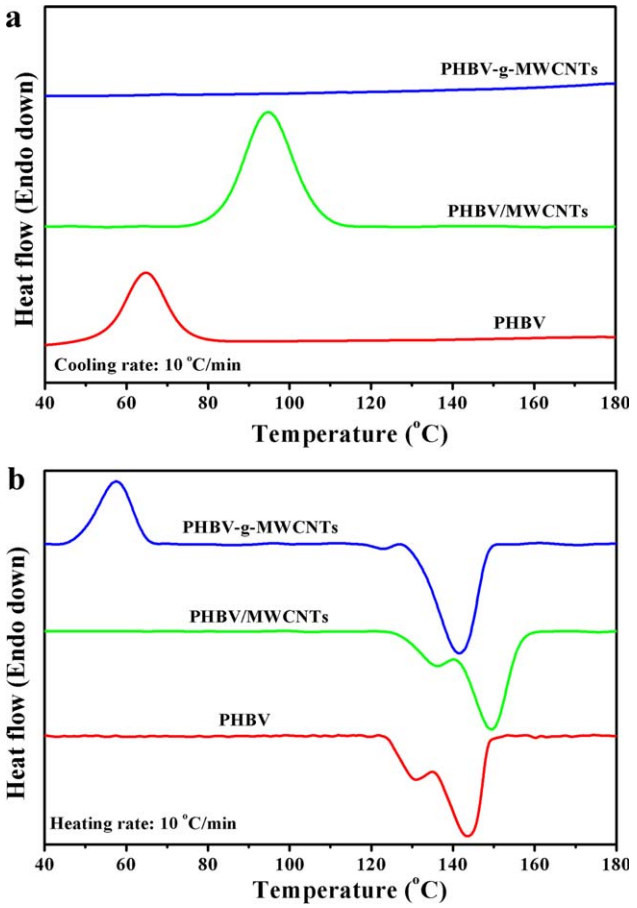

Figure 4. DSC traces of the PHBV, PHBV/MWCNTs, and PHBV-*g*-MWCNTs at a rate of 10°C/min: (a) the first cooling scan and (b) the second heating scan. [Color figure can be viewed in the online issue, which is available at wileyonlinelibrary.com.]

second heating traces. Double or multiple melting behaviors of the PHBV and PHBV/MWCNT nanocomposites have been reported.[8,16,18,19] This study revealed that this complex double melting behavior of PHBV and its nanocomposites could have been due to the reorganization of crystals through a melting and recrystallization mechanism during subsequent DSC heating; we differentiated between them by simply varying β.[8,16] Compared with that of PHBV, the higher melting temperature (T_{m2}) of PHBV/MWCNTs increased by 5.9°C from 143.7 to 149.6°C but decreased to 141.5°C for PHBV-*g*-MWCNTs (as shown in Table I). This illustrated that the crystal perfection of the PHBV/MWCNTs was improved, but imperfect crystals with a confined structure appeared in the PHBV-*g*-MWCNTs because of the occurrence of MWCNTs; we demonstrate this in detail in the following parts. Moreover, a new cold crystallization peak appeared at 57.8°C for the PHBV-*g*-MWCNTs during the second heating traces, as shown in Figure 4(b). However, no crystallization peaks were found in the original PHBV or the PHBV/MWCNTs. This hinted that a strong constraint to the crystallization of PHBV occurred because of the limited segmental mobility of PHBV grafted onto the surface of the MWCNTs.

Effect of the Cooling Rates and βs on the Cold Crystallization Behavior

The exothermic peak during the heating scan of DSC analysis is called the *cold crystallization peak* and originated from the crystallization of the amorphous regions. The cold crystallization behavior of the PHBV-*g*-MWCNTs was further studied by variation of the cooling rates and βs from 2 to 20°C/min. Figure 5(a) shows that with the increase of the cooling rates, no obvious melt crystallization peak appeared in the PHBV-*g*-MWCNTs at the higher cooling rate (>2°C/min); even at a slow cooling rate, only a weak crystallization peak of 45.2°C was

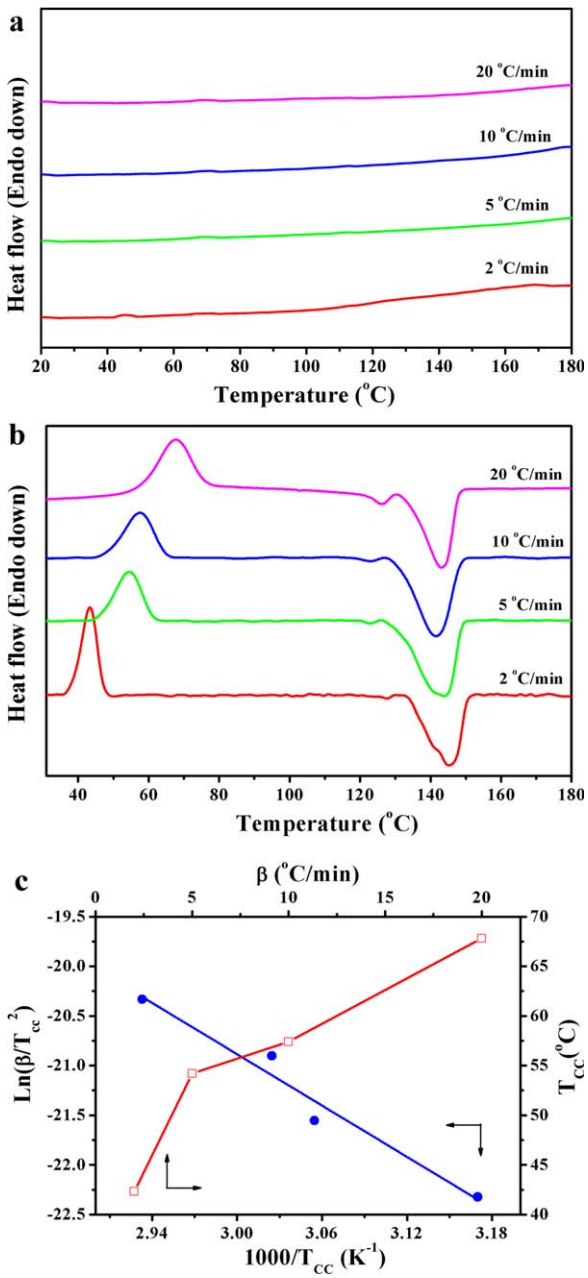

Figure 5. DSC traces at various (a) cooling rates and (b) βs ranging from 2 to 20°C/min and (c) T_{cc} and Kissinger's plots as a function of the βs for the PHBV-*g*-MWCNTs. [Color figure can be viewed in the online issue, which is available at wileyonlinelibrary.com.]

observed. This indicated that it was difficult to form the effective crystallization nuclei on the cooling traces at different rates, even with enough incubation time to nucleate at a slow cooling rate; this was ascribed to the strong confinement of the PHBV chain segments by the grafting of the MWCNTs. Moreover, with increasing β, the melting peaks became wider and shifted toward lower temperatures, whereas the cold crystallization peaks became wider and shifted toward higher temperatures, as shown in Figure 5(b). The changes in the peaks position, height, and shape with the pretreatment history reflected the corresponding changes in the amorphous regions. As β increased, the time available for a desired temperature to be reached was reduced, and thus, crystallization lagged and was initiated at a relatively high temperature. Thus, it was revealed that the MWCNTs could exert an influence on the amorphous region of PHBV during the pretreatment stage because the cold crystallization peak originated from the crystallization of the remaining amorphous regions after thermal treatment, and the cold crystallization behavior of PHBV was related to the temperature dependence of nucleation and chain diffusion.

The effect of β on the variation of the cold crystallization temperature (T_{cc}) of PHBV-*g*-MWCNTs is summarized in Figure 5(c). T_{cc} increased with increasing β because we know that glasses need to undergo structural relaxation, through which they can transform from a metastable state to a stable state during crystallization. The transformation had less time to crystallize in a low crystallization range with increasing β; this prevented the entire energy of structural relaxation from being released. Therefore, T_{cc} shifted to a high and wide temperature range. The activation energy of cold crystallization (E_{cc}) was calculated with the Kissinger formula,[23] which is most commonly used in the analysis of crystallization data. This formula for the general case can be expressed as follows:

$$\ln\left(\frac{\beta}{T^2 cc}\right) = -\frac{E_{cc}}{RT_{cc}} + \text{const} \quad (1)$$

where R is the universal gas constant and T_{cc} is the crystallization's peak temperature. The value of E_{cc} was obtained from the slope of ln (β/T_{cc}^2) versus $1/T_{cc}$ plot; this is the activation energy required to transport the molecular segments to the crystallization surfaces. The smaller E_{cc} is, the more easily the polymer crystallizes.[23] The value of the activation energy was 71.7 kJ/mol for PHBV-*g*-MWCNTs according to Kissinger formula; this was larger than the activation energy of PHBV (ca. 43.5 kJ/mol). These results indicate that there must have been some conformational and structural changes for PHBV grafted onto the MWCNTs; this resulted in the restricted mobility of chain segments.

Isothermal Crystallization Morphologies

The polarized optical microscopy of the crystals produced by the crystallization of the neat PHBV, PHBV/MWCNTs, and PHBV-*g*-MWCNTs at an isothermal crystallization temperature of 45°C was performed in our experiment. As shown in Figure 6, the size of the PHBV spherulites (ca. 40 μm in diameter) was large because of the low nucleation density of PHBV, as shown in Figure 6(a). With the addition of the CNTs, the size of the spherulites became smaller in the PHBV/MWCNTs, as shown in Figure 6(b), because the nucleation density of the crystals was much higher than that of PHBV. The radial growth of numerous spherulites in the nanocomposites based on CNT nuclei ceased after the surfaces of the PHBV spherulites came into contact each other; this was believed to the confined crystallization constructed by the CNT filler.[16] However, Figure 6(c) shows that broken and imperfect spherulites were found for the PHBV-*g*-MWCNTs, and thus, the spherulites sizes could not be calculated. In addition, when the time was prolonged, the crystal growth of the spherulites was still very slow, and the spherulites could not connect together just like the PHBV/MWCNTs [Figure 6(b)]. Such results indicated that the noncovalent interactions of the CNTs in the nanocomposite reduced the size of spherulites and facilitated the overall crystallization rate and provided heterogeneous nucleation sites for the crystallization of PHBV; this could be attributed to both the heterogeneous nucleation effect and confined crystallization of the PHBV chains through the addition of CNTs. However, the covalent

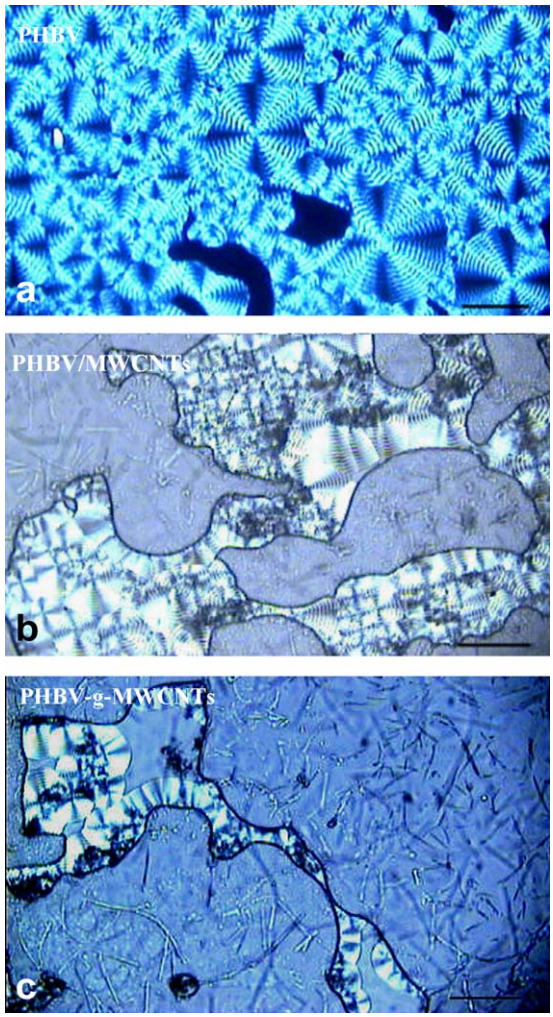

Figure 6. Optical micrographs of the spherulitic morphologies of the neat PHBV, PHBV/MWCNTs, and PHBV-*g*-MWCNTs (same magnification, scale bar = 50 μm). [Color figure can be viewed in the online issue, which is available at wileyonlinelibrary.com.]

Applied Polymer SCIENCE

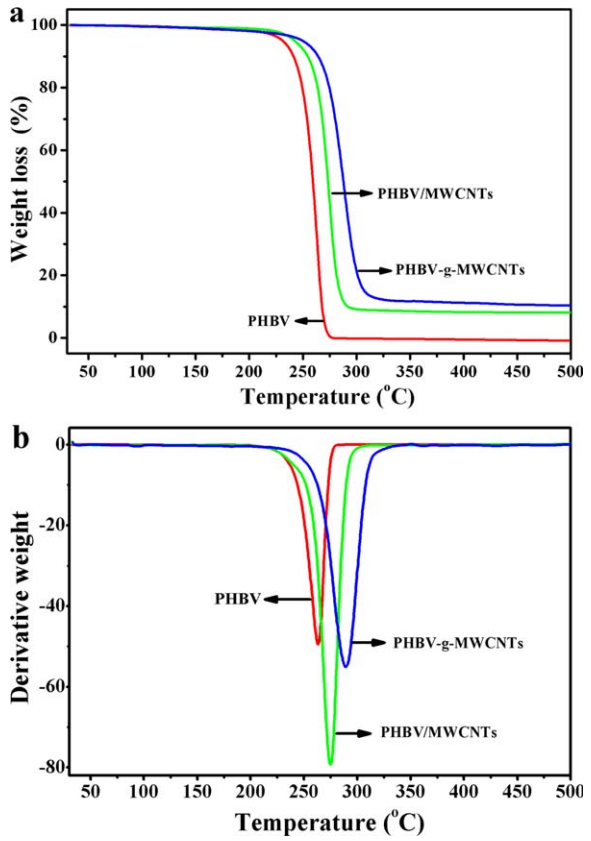

Figure 7. (a) TGA and (b) corresponding derivative thermogravimetry curves of the neat PHBV, PHBV/MWCNTs, and PHBV-*g*-MWCNTs. [Color figure can be viewed in the online issue, which is available at wileyonlinelibrary.com.]

interactions of the MWCNTs restricted the conformational and structural changes of the PHBV chains to result in the confined crystal structure or imperfect spherulites of PHBV in the nanocomposite during crystallization; this was consistent with the WAXD and DSC results.

Thermal Stability

One of the main disadvantages of biodegradable PHBV is its low thermal stability due to its serious thermal degradation during polymer melt processing. The addition of the MWCNTs resulted in an improvement in the heat resistance of the polymer matrix because of the inherent high thermal stability of the MWCNTs, as shown in Figure 7(a). The maximum decomposition temperature (T_{max}) shifted to a higher temperature in both the PHBV/MWCNTs and PHBV-*g*-MWCNTs. There was a single peak with a T_{max} appearing in the derivative thermogravimetry curves for all of the samples, as shown in Figure 7(b); this indicated that the thermal degradation of PHBV with or without MWCNTs was carried out by one-step traces. It is well known that PHBV undergoes both random chain scission and specific chain-end scission simultaneously at a lower temperature; this is probably random chain cleavage via cis elimination.[19] However, with the introduction of the CNTs, the transport of combustion gas, such as carbon dioxide, was hindered, and the absorption of free radicals generated during polymer decomposition by the activated carbon surface,[8] a significant improvement in the thermal stability in the PHBV/MWCNTs and PHBV-*g*-MWCNTs, was observed. Table I lists the characteristic parameters in the thermal degradation traces of the neat PHBV, PHBV/MWCNTs, and PHBV-*g*-MWCNTs. Compared with those of PHBV, the initial decomposition temperature (T_0), the temperature determined at 5% weight loss ($T_{5\%}$), T_{max}, and the complete decomposition temperature (T_f) for the PHBV-*g*-MWCNTs increased by amplitudes of 19.3, 18.0, 23.7, and 32.9°C, respectively. A significant improvement in the thermal stability was benefited from the formation of covalent bonds between the PHBV and MWCNTs. T_{max} of the PHBV-*g*-MWCNTs was improved by about 14.4°C compared with that of the PHBV/MWCNTs and by about 23.7°C compared with that of the original PHBV. In addition, the $T_0 - T_{m2}$ values of the PHBV, PHBV/MWCNTs, and PHBV-*g*-MWCNTs were calculated and are listed in Table I; this reflects the melt-processing window. Generally, the larger the $T_0 - T_{m2}$ value of a polymer is, the wider the melt-processing window of polymer is. As shown in Table I, the $T_0 - T_{m2}$ value of the PHBV-*g*-MWCNTs was 129.3°C; this was higher than the 112.6°C for the PHBV/MWCNTs and the 107.8°C for the neat PHBV. This result illustrated that the PHBV-*g*-MWCNTs exhibited the widest melt-processing window among them.

CONCLUSIONS

Poly(3-hydroxybutyrate-*co*−3-hydroxyvalerate) (PHBV) molecules were either chemically bonded or physically blended on MWCNTs to directly compare the influence of the interactions types on the microstructure and properties of the resulting nanocomposites. The PHBV-*g*-MWCNTs were prepared through an esterification reaction between the carboxylic groups of the MWCNTs and the hydroxyl groups of PHBV; they exhibited a clear core–shell structure composed of MWCNTs with an average diameter of 30 nm as a hard core and a PHBV layer with an average thickness of 60 nm as a soft shell. We found that compared with those of PHBV, because of the limited segmental mobility of the polymer grafted onto the surface of the MWCNTs, the nonisothermal crystallization of the PHBV-*g*-MWCNTs was markedly hindered, and this exhibited an exothermic cold crystallization peak at 57.8°C and a decrease in X_c. However, the crystallization for PHBV in the PHBV/MWCNT nanocomposite was enhanced, and X_c significantly increased due to a heterogeneous nucleation effect of the MWCNTs. The thermal stability of the composites containing covalently functionalized nanotubes was enhanced greatly relative to the noncovalent ones because of the stronger nanotube/polymer interaction. The T_{max} of the PHBV-*g*-MWCNTs was improved by about 14.4°C compared with that of the PHBV/MWCNT composite and by about 23.7°C compared with that of the original PHBV. Moreover, the $T_0 - T_{m2}$ value of the PHBV-*g*-MWCNTs was higher than those of the PHBV/MWCNTs and original PHBV; this indicated that the PHBV-*g*-MWCNTs had the widest melt-processing window. Some of the disadvantages of PHBV were overcome by the covalent grafting of the MWCNTs onto the PHBV segments; this could extend its application to ecofriendly and biomedical materials. Further work is needed to understand the CNT-induced PHBV crystallization

and make comparisons with PHBV/MWCNTs and PHBV/PHBV-*g*-MWCNT composites.

ACKNOWLEDGMENTS

This work was supported by the Program for New Century Excellent Talents in University (contract grant number NCET070763), the Key Basic Research Foundation of the Committee of Science and Technology of Shanghai Municipality (contract grant number 06JC14003), the Fundamental Research Funds for the Central Universities, and the Doctorate Innovation Foundation of Donghua University (contract grant number BC201101).

REFERENCES

1. Hazer, D. B.; Kilicay, E.; Hazer, B. *Mater. Sci. Eng. C* **2012**, *32*, 637.
2. Hazer, B. *Int. J. Polym. Sci.* **2010**, *2*, 31.
3. Arslan, H.; Menteş, A.; Hazer, B. *J. Appl. Polym. Sci.* **2004**, *94*, 1789.
4. Hazer, B.; Steinbüchel, A. *Appl. Microbiol. Biotechnol.* **2007**, *74*, 1.
5. Qu, X.; Wu, Q.; Zhang, K.; Chen, G. *Biomaterials* **2006**, *27*, 3540.
6. Sun, J.; Wu, J.; Li, H.; Chang, J. *Eur. Polym. J.* **2005**, *41*, 2443.
7. Cool, S.; Kenny, S.; Wu, A.; Nurcombe, V.; Trau, M.; Cassady, A.; Grondahl, L. *J. Biomed. Mater. Res. A* **2007**, *82*, 599.
8. Lai, M.; Li, J.; Yang, J.; Liu, J.; Tong, X.; Cheng, H. *Polym. Int.* **2004**, *53*, 1479.
9. Xu, C.; Qiu, Z. *Polym. Adv. Technol.* **2011**, *22*, 538.
10. Chan, K. H. K.; Wong, S. Y.; Tiju, W. C.; Li, X.; Kotaki, M.; He, C. B. *J. Appl. Polym. Sci.* **2010**, *116*, 1030.
11. Liu, L.; Etika, K. C.; Liao, K. S.; Hess, L. A.; Bergbreiter, D. E.; Grunlan, J. C. *Macromol. Rapid. Commun.* **2009**, *30*, 627.
12. Sanchez-Garcia, M.; Lagaron, J.; Hoa, S. *Compos. Sci. Technol.* **2010**, *70*, 1095.
13. Zhao, Y.; Wang, S.; Guo, Q.; Shen, M.; Shi, X. *J. Appl. Polym. Sci.* **2013**, *127*, 4825.
14. Yoon, J. T.; Jeong, Y. G.; Lee, S. C.; Min, B. G. *Polym. Adv. Technol.* **2009**, *20*, 631.
15. Kim, H.; Park, B.; Yoon, J.; Jin, H. *Eur. Polym. J.* **2007**, *243*, 1729.
16. Shan, G. F.; Gong, X.; Chen, W. P.; Chen, L.; Zhu, M. F. *Colloid Polym. Sci.* **2011**, *289*, 1005.
17. Xu, C.; Qiu, Z. *J. Polym. Sci. Part B: Polym. Phys.* **2009**, *47*, 2239.
18. Yu, H. Y.; Qin, Z. Y.; Wang, L. F.; Zhou, Z. *Carbohydr. Polym.* **2012**, *87*, 2447.
19. Liu, Q. S.; Zhu, M. F.; Wu, W. H.; Qin, Z. Y. *Polym. Degrad. Stab.* **2009**, *94*, 18.
20. Yamane, H.; Terao, K.; Hiki, S.; Kimura, Y. *Polymer* **2001**, *42*, 3241.
21. Ublekov, F.; Baldrian, J.; Nedkov, E. *J. Polym. Sci. Part B: Polym. Phys.* **2009**, *47*, 751.
22. Lee, J. C.; Yasui, A.; Jeong, Y.; Sakurai, S.; Yamane, H. *Polymer* **2008**, *49*, 2362.
23. Liu, Q. S.; Deng, B. Y.; Tung, C. H.; Zhu, M. F.; Shyr, T. W. *J. Polym. Sci. Part B: Polym. Phys.* **2010**, *48*, 2288.